micromachines

MDPI

Article

An Investigation on CCT and Ra Optimization for Trichromatic White LEDs Using a Dual-Weight-Coefficient-Based Algorithm

Hua Xiao [1,2,*], Yan Li [3], Binghui Li [4] and Guancheng Wang [1]

1 School of Electronic and Information Engineering, Guangdong Ocean University, Zhanjiang 524088, China; wanggc@gdou.edu.cn
2 Technology Development Centre, Shenzhen Institute of Guangdong Ocean University, Shenzhen 518120, China
3 Research and Development Center for Solid State Lighting, Institute of Semiconductors, Chinese Academy of Sciences, Beijing 100083, China; yanli7@semi.ac.cn
4 Shenzhen Institute of Artificial Intelligence and Robotics for Society (AIRS), The Chinese University of Hong Kong (CUHK), Shenzhen 518000, China; libinghui@cuhk.edu.cn
* Correspondence: oliviaxh@gdou.edu.cn

Abstract: Spectral optimization is applied as an effective tool in designing solid-state lighting devices. Optimization speed, however, has been seldomly discussed in previous reports as regards designing an algorithm for white light-emitting diodes (WLEDs). In this study, we propose a method for trichromatic WLEDs to obtain the optimal Ra under target correlated color temperatures (CCTs). Blue-, yellow-, and red-color monochromatic spectra, produced by the GaN LED chip, YAG:Ce^{3+} phosphors, and CdSe/ZnSe quantum dots, respectively, are adopted to synthesize white light. To improve the effectiveness of our method, the concept of dual weight coefficients is proposed, to maintain a numerical gap between the proposed floating CCT and the target CCT. This gap can effectively guarantee that Ra and CCT ultimately move toward the targeting value simultaneously. Mechanisms of interaction between CCT, Ra, and dual-weight coefficients are investigated and discussed in detail. Particularly, a fitting curve is drawn to reveal the linear relationship between weight coefficients and target CCTs. This finding effectively maintains the accuracy and accelerates the optimization process in comparison with other methods with global searching ability. As an example, we only use 29 iterations to achieve the highest Ra of 96.1 under the target CCT of 4000 K. It is hoped that this study facilitates technology development in illumination-related areas such as residential intelligent lighting and smart planting LED systems.

Keywords: light-emitting diode; spectral optimization; correlated color temperature (CCT); general color rendering index (Ra)

Citation: Xiao, H.; Li, Y.; Li, B.; Wang, G. An Investigation on CCT and Ra Optimization for Trichromatic White LEDs Using a Dual-Weight-Coefficient-Based Algorithm. *Micromachines* **2022**, *13*, 276. https://doi.org/10.3390/mi13020276

Academic Editors: Wei Chen and Junjie Hao

Received: 13 January 2022
Accepted: 31 January 2022
Published: 9 February 2022

1. Introduction

In comparison with RGB LEDs, light-conversion-material-based white light-emitting diodes (WLEDs) have played leading roles in solid-state illumination, due to their high light-conversion efficiencies in specific wavebands, stability under various junction temperatures, low cost, and feasibility in color tunability [1–3]. Conventionally, the color performance of WLEDs is evaluated from two aspects: the emitting color from the WLED and the releasing color of objects exposed under the WLED. Theoretically, the former is characterized by correlated color temperature (CCT), and the latter is characterized by color rendering property, in which the concept of general color rendering index (Ra) is conventionally adopted for evaluation by the International Commission on Illumination [4]. CCT expresses a warm or cold feeling when we observe the light beam, while Ra reveals the ability of a light source to express the real color of an object. Ra represents the average value of the color rendering index (CRI) of eight general colors in a WLED system. CCT and Ra are functions of monochromatic spectral power distributions (SPDs) of different colors [5]. Therefore, if we intend to adjust the circadian rhythm of humans and plantings or reduce driver's fatigue in a specific scenario, modulating the SPD of the WLED system is effective and indispensable [6]. In trichromatic WLEDs, the white-light SPD ($SPD_W(\lambda)$) is conventionally generated by downconverting light-conversion materials with blue LED chips, in which light in short wavebands (such as blue light) can be effectively converted to light in long wavebands (such as red light) under the stokes effect.

In the last few decades, SPD optimization technologies have been widely investigated to facilitate illumination in areas of residential lighting [7], agriculture [8], rehabilitation therapy [9], and visible light communication [10,11]. These technologies can be mainly divided into two catalogs: the first type is to optimize the color rendering property and energy consumption by adjusting peak wavelengths, spectral bandwidth, and intensity by using Gaussian functions; the other is to optimize the color rendering property and energy consumption by adjusting the density of real light in different colors. For the first type, Guo et al. [12] conducted comprehensive numerical simulations of three-hump and four-hump SPDs in WLEDs. The changes in Ra and CCT values with the shifting peak wavelengths of full width at half maximums (FWHMs) were analyzed under different operating temperatures. The relationship between scotopic–photopic ratio and CCT was investigated as well. Wei et al. [13] proposed six-channel-based LEDs to synthesize daylight with high quality by using a genetic algorithm and Gaussian spectral model. For the second type, Zhu et al. [14] conducted a comprehensive study on illumination performances of the perovskite-based LED with four humps. Titkov et al. [15] proposed a semi-hybrid device, which combined monolithic blue-cyan LED with green-red phosphor mixture, exhibiting the highest Ra of 98.6 at CCT of 3400 K. Yuan et al. [16] manufactured a trichromatic WLED, which constitutes of blue-pump carbon dots and phosphor glass, realizing the highest Ra of 92.9 at CCT of 3610 K. Among these studies, a variety of methods are conventionally used, such as the multiple Gaussian function method [17], least-squares method [18], and iterative method of gradient descent [19]. However, these methods focus on improving the accuracy and the feasibility, as well as developing light-conversion material species with superior chromaticity; few of them discuss the improvement strategy of optimization speed for WLEDs.

With the development of the Internet of Things (IoT) and 5G technologies, the intelligent control technology of illumination lamps becomes imperative for saving energy and increasing productivity [20,21]. Therefore, improving the effectiveness of spectral optimization becomes a key issue in intelligent control. In this study, we propose a convenient method to optimize CCT and Ra values simultaneously for trichromatic WLEDs by using dual-weight coefficients. These coefficients can effectively control the variation range of CCT while searching for the optimal Ra value. Key steps to realize the proposed method is analyzed comprehensively. Compared with other conventional methods used for spectral optimization, the proposed method can greatly accelerate the calculation process while maintaining accuracy.

2. Monochromatic Spectra Preparation and Theory of Algorithms

As shown in Figure 1a, the blue-emissive LED chip (302 × 198 μm^2, Hualian Co., Ltd., Xiamen, China) was selected as the excitation source, and yellow-emissive cerium-doped yttrium aluminum garment phosphors ($YAG:Ce^{3+}$, Youyan Rare Earth Co., Ltd., Beijing, China) and red-emissive CdSe/ZnSe quantum dots (Poly OptoElectronics Co., Ltd., Jiangmen, China) were selected as light-conversion materials to fabricate white light. $YAG:Ce^{3+}$ phosphors can greatly broaden the white-light spectrum in the visible-light regime, while CdSe/ZnSe quantum dots are able to provide pure red emission with high stability and high quantum yields (QYs). Recently, QYs of $YAG:Ce^{3+}$ phosphors and CdSe/ZnSe quantum dots can reach up to 90% and ~100%, respectively [22,23]. Packaging technology of the WLED has been given in [24]. To facilitate our study, spectra of monochromatic blue, yellow, and red light are referred to as $SPD_B(\lambda)$, $SPD_Y(\lambda)$, and $SPD_R(\lambda)$, respectively.

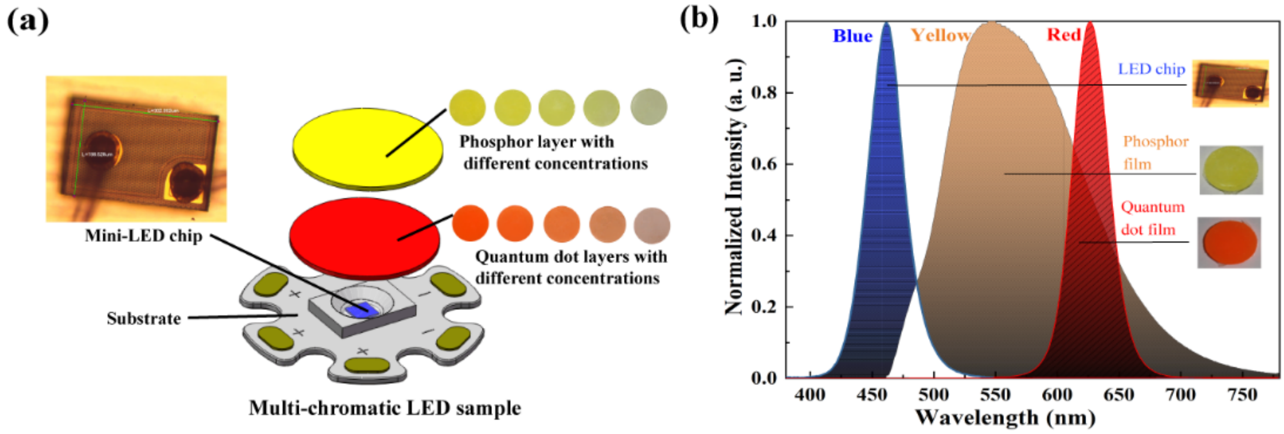

Figure 1. (**a**) The assembly of the trichromatic LED sample and (**b**) monochromatic spectra of blue, yellow, and red light, which produced by LED chip, YAG:Ce^{3+} phosphors, and Cdse/ZnSe quantum dots, respectively.

A 500 mm diameter-integrating sphere (Everfine) was utilized to measure $SPD_B(\lambda)$. To obtain $SPD_Y(\lambda)$ and $SPD_R(\lambda)$, we mathematically removed the superposition area of blue light of the original emission spectra produced by phosphors and quantum dots [24]. $SPD_B(\lambda)$, $SPD_Y(\lambda)$, and $SPD_R(\lambda)$ were normalized before optimization. From Figure 1b, we observe that the LED chip and CdSe/ZnSe quantum dots generate narrow blue and red peaks with FWHM of 54 nm and 56 nm, respectively. On the other hand, YAG:Ce^{3+} phosphors produce a spectrum with FWHM of 125 nm that covers a wide range of visible light. Here, we assumed that the peak wavelength and the FWHM of these monochromatic spectra are independent of the driven current, so $SPD_W(\lambda)$ can be described as a linear combination of $SPD_B(\lambda)$, $SPD_Y(\lambda)$, and $SPD_R(\lambda)$, as described by

$$SPD_W(\lambda) = A_B \cdot SPD_B(\lambda) + A_Y \cdot SPD_Y(\lambda) + A_R \cdot SPD_R(\lambda) \quad (1)$$

where A_B, A_Y, and A_R are the proportions of the radiant power of blue, yellow, and red light, respectively.

Before calculation, target CCT, test CCT, and test Ra values are defined as CCT_{tar}, CCT_{test}, Ra_{test}, respectively. CCT_{test} and Ra_{test} represent current CCT and Ra values in the calculation. Figure 2a illustrates the steps for spectral optimization using the proposed method. For comparison, conventional methods I and II used for spectral optimization are illustrated in Figure 2b,c. Among these three methods, method I directly considers all the possibilities of A_B, A_Y, and A_R under CCT_{tar}, while method II randomly selects values of A_B, A_Y, and A_R until fulfilling the cycle index, which is set as 1000 for methods I and II. Both methods I and II use the bubbling method to obtain the highest Ra within the error range of CCT_{tar}. For the proposed method, the calculation steps are described as follows:

(1) First, we initialize the procedure and load original data, such as the spectra of monochromatic light, step lengths for iteration, error ranges of Ra and CCT, and initial values of A_B, A_Y, and A_R;
(2) Two key problems for CCT optimization are how to adjust CCT_{test} and how to optimize Ra in the meantime. According to the relationship between CCT and components of different colors, we first set a floating parameter between the initial CCT and CCT_{tar}, which is named CCT_m. The relationship between CCT_m and CCT_{test} can be expressed as $CCT_{test} = \delta_1 + CCT_m$, where δ_1 is the first weight coefficient in our algorithm. To realize CCT_m, we only need to modulate the parameter of A_B;
(3) Before realizing CCT_{tar}, we optimize Ra_{test} by using the bubbling method. Keeping the proportion of A_B and A_Y unchanged, we attempt to modulate A_R with a small step to observe the change of Ra_{test}. If the small step helps to increase the value of Ra, we conduct a similar iteration until Ra_{test} reaches the highest value; otherwise, we

modulate A_R in the negative direction. The relationship between CCT_m and CCT_{tar} can be expressed as $CCT_{tar} = \delta_2 + CCT_m$, where δ_2 is the second weigh coefficient in our algorithm.

(4) When the calculation result meets the required conditions, we export optimized A_B, A_Y, and A_R values, the optimized WLED spectra, CCT_{test}, as well as Ra_{test}.

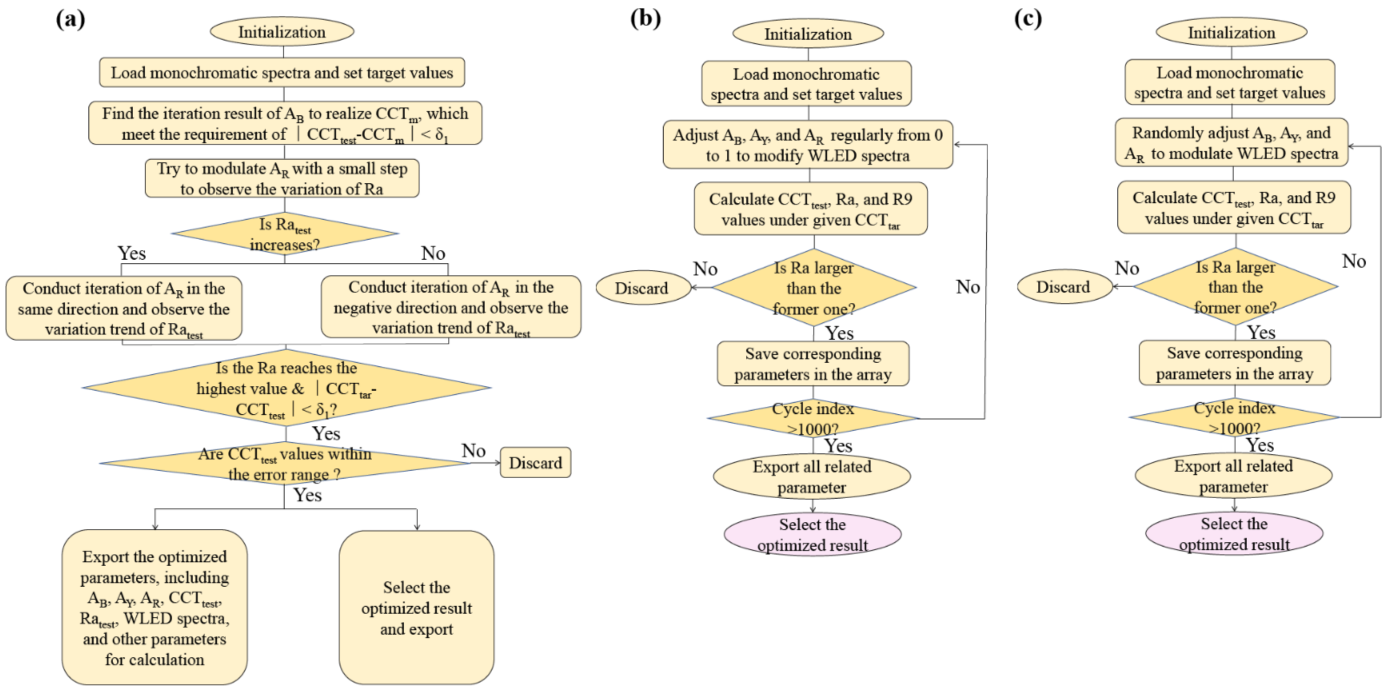

Figure 2. Flow diagrams of (**a**) the proposed method, (**b**) method I, and (**c**) method II, in which methods I and II are conventionally used for spectral optimization.

Below is the design philosophy of the proposed algorithm. Particularly, we propose a floating CCT value named CCT_m and two weight coefficients, named δ_1 and δ_2, to control the variation range of the CCT_{test}. There exist two main stages in the optimization process: We first impel CCT_{test} to move toward CCT_m and then optimize Ra_{test} and CCT_{test} simultaneously, to reach the optimum Ra and CCT_{tar}. If we directly search for CCT_{tar}, the variation space of Ra_{test} is very limited, due to the interaction effect of CCT and Ra. The proposal of CCT_m can effectively solve this problem, rendering CCT_{test} reach a position near CCT_{tar} before the optimization of Ra_{test}.

Weight coefficients of δ_1 and δ_2, which determine the value of CCT_m and the shifting range of CCT_{test}, are key for the optimization result. If δ_2 is too small, Ra_{test} will not reach the highest value due to the limited shifting space; on the other hand, if δ_2 is too large, Ra_{test} can reach the highest value soon but at the expense of the error between CCT_{test} and CCT_{tar}. Another problem is how to guarantee that CCT_{test} moves toward CCT_{tar} instead of the reverse direction while optimizing Ra_{test}. To solve this problem, we set the original A_B, A_Y, and A_R values as 0.1, 0.3, and 0.5, respectively, in which A_R is large enough to guarantee the decreasing trend of A_R while optimizing Ra_{test}.

3. Results and Discussion

3.1. Relationship between CCT, Ra, and Other Parameters

Figure 3 illustrates the variation of CCT_{test}, Ra_{test}, and δ_1 under different δ_2 in a 3D coordinate diagram, when CCT_{tar} is set as 8000 K. To facilitate discussion, these results are separately presented in Figure 3a,b at different view angles. In Figure 3a, CCT_{test} is decreasing with the increase in δ_1 when δ_2 equals 3000 K. The reason is that δ_1 directly influences the difference between CCT_{test} and CCT_m. If δ_1 is too large, CCT_{test} becomes much smaller than CCT_m, increasing the difficulty of reaching CCT_{tar} while optimizing Ra_{test}. According to the methodology of the algorithm, optimization will finally stop when we obtain the optimal Ra. By then, the final CCT_{test} obtained may fail to reach CCT_{tar}.

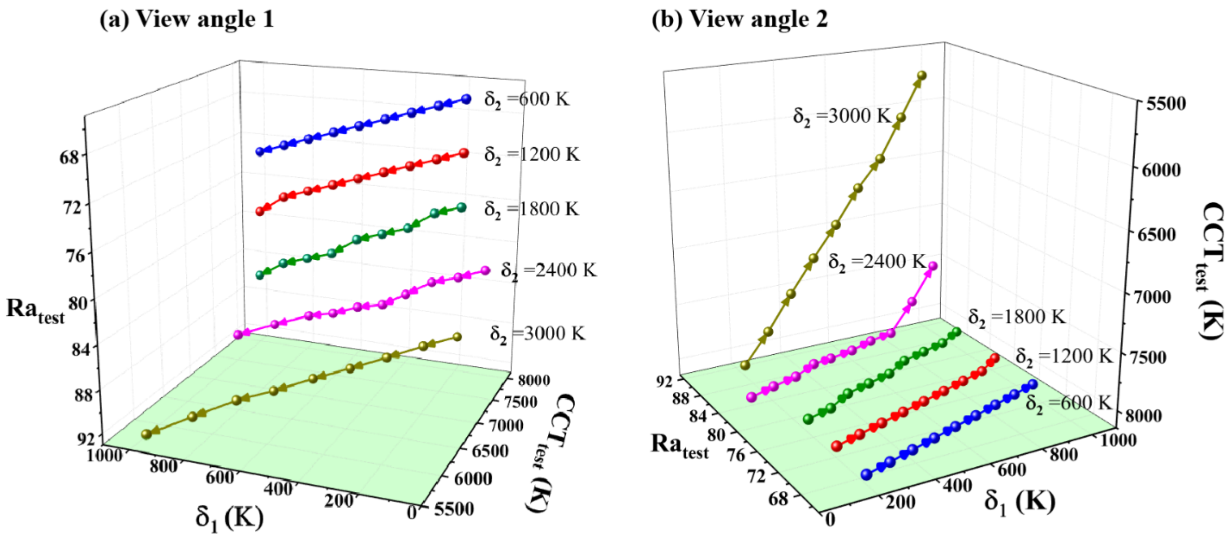

Figure 3. Shifting trend of CCT_{test}, Ra_{test}, and δ_1 under different δ_2 in a 3D coordinate diagram with CCT_{tar} of 8000 K. (**a**,**b**) are the same 3D figure at different view angles.

Secondly, Ra_{test} increases with the increase in δ_2. Since δ_2 represents the difference between CCT_m and CCT_{tar}, when we increase δ_2, CCT_m becomes smaller. Thus, larger δ_2 provides a wider range for Ra optimization, extending the shifting area of Ra_{test} within the permitted range of CCT_{test}.

From Figure 3b, we observe the variation of CCT_{test}, Ra_{test}, and δ_1 under different δ_2 at the other view angle. When δ_2 is set as 600 K, 1200 K, and 1800 K, respectively, the curves almost lie in a similar plane with CCT_{tar}, equal to 8000 K. However, for δ_2 = 2400 K and δ_2 = 3000 K, corresponding curves stretch out of this plane. In other words, their CCT_{test} become much smaller than CCT_{tar} of 8000 K. Below are the explanation for this phenomenon. For δ_2 = 2400 K and δ_2 = 3000 K, we reserve a large variation range of CCT to support the optimization for CCT_m and Ra_{test}, causing the inaccessibility of CCT_{tar} when the optimization process of Ra is ending. This explains the phenomenon that those points on the curve are almost far away from 8000 K when δ_2 = 3000 K. When δ_2 decreases from 3000 K to 2400 K, a portion of points on the curve return to the plane of 8000 K. To summarize, those points staying near the plane of 8000 K are constrained by CCT_{tar}; those points that stretch out from the plane of 8000 K are constrained by optimization conditions of Ra.

As shown in Figure 4a, R_{atest} increases with an increase in δ_1 and δ_2. If δ_1 remains unchanged and δ_2 decreases, it would cost more iteration steps to increase A_B in order to improve CCT_{test}. Hence, even CCT_{test} reaches CCT_m; however, the value of A_B already becomes very large, which limits the highest Ra the WLED can realize. As lower A_B helps the prompt enhancement of Ra_{test}, overlarge A_B hinders the improvement of Ra_{test}, despite the adjustment of A_R. On the other hand, if we keep δ_2 unchanged and decrease δ_1, CCT_{test} will reach CCT_m sooner; however, Ra_{test} cannot be fully optimized. Therefore, the value of optimal A_B is influenced by CCT_m and is finally determined by δ_1 and δ_2. Increasing δ_1 and δ_2 under high CCT_{tar} can greatly decrease CCT_m, enlarging the optimization range of Ra. In Figure 4b, CCT_{test} slightly decreases when we increase δ_1 or δ_2, indicating that CCT_{test} has a reverse shifting trend, compared with Ra_{test} under different δ_1 and δ_2 values.

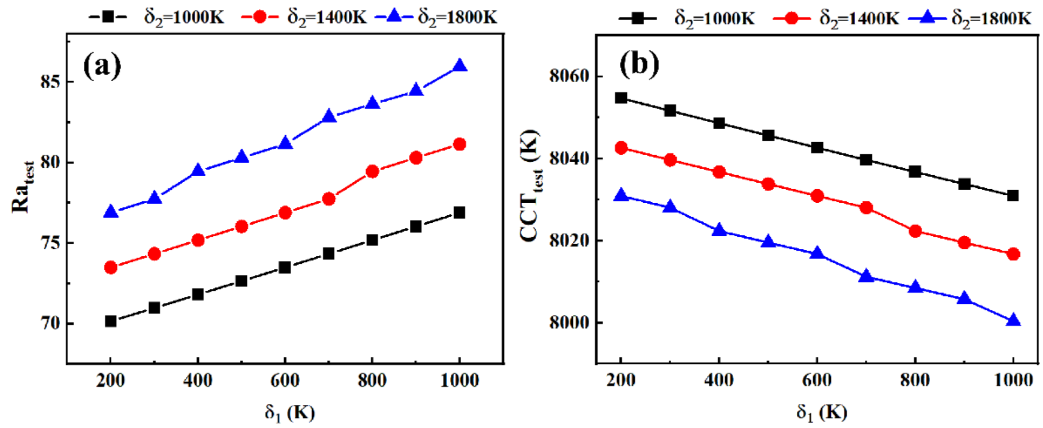

Figure 4. (**a**) Variation in Ra_{test} under different δ_1 values, when δ_2 equals to 1000 K, 1400 K, and 1800 K, respectively; (**b**) variation in CCT_{test} under different δ_1 values, when δ_2 equals to 1000 K, 1400 K, and 1800 K, respectively.

These analyses reveal the significance of δ_1 and δ_2 for the optimization result. The WLED with different CCT_{tar} values has different reactions under similar δ_1 and δ_2. Thus, balancing the relationship between δ_1, δ_2, and CCT_{tar} is the next step to accelerate the optimization process.

Figure 5a illustrates the optimized spectra of the trichromatic WLED under conditions of CCT_{tar} = 8000 K and δ_1 = 200 K. When δ_2 increases from 600 K to 3000 K, peaks of blue and red light slightly decrease, while Ra_{test} increases from 66.9 to 89.7. This is because the WLED spectrum is increasingly close to the spectrum of the reference source (black body source) [14]. The shifting trend of Ra_{test} matches well with the analysis results of Figure 3a.

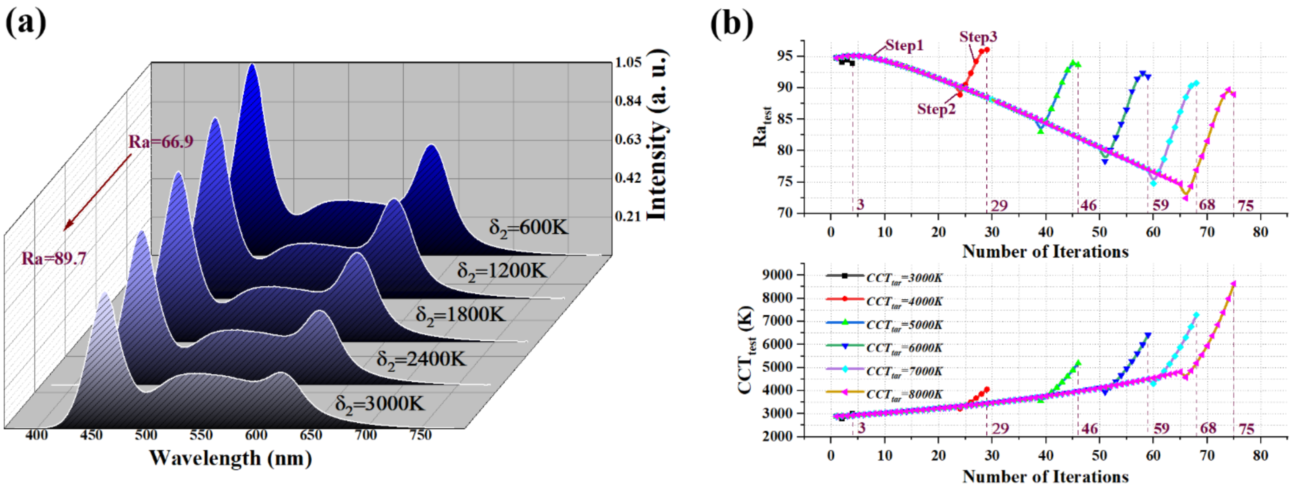

Figure 5. (**a**) The optimized spectra of the trichromatic WLED under the condition of CCT_{tar} of 8000 K and δ_1 of 200 K. (δ_2 is ranging from 600–3000 K); (**b**) the shifting trend of iterations of CCT_{test} and Ra_{test} under different CCT_{tar} values.

Figure 5b describes the shifting trend of CCT_{test} and Ra_{test} in the iteration process under various CCT_{tar} values. When CCT_{tar} ranges from 4000 K to 8000 K, Ra_{test} declines slowly at first, as shown in step 1; thereafter, Ra_{test} abruptly decreases in a small step, as shown in step 2; finally, Ra_{test} increases severely until reaching the top point before finishing the optimization steps, as shown in step 3. With the increase in CCT_{tar}, the highest value of Ra that can be achieved decreases. A similar phenomenon has been observed in [24,25].

When CCT_{tar} ranges from 4000 K to 8000 K, CCT_{test} also shows three steps to reach CCT_{tar}; however, the shifting trend of CCT_{test} during the optimization process is different from that of Ra_{test}. Ra_{test} decreases slowly at first and then increases drastically; on the other hand, CCT_{test} increases slowly at first and then increases drastically. A comparison of Figure 5a with Figure 5b indicates that the increase in CCT_{test} in step1 sacrifices the improvement of Ra_{test} in the initial time. In step 3, different from the optimization aim of Ra_{test}, we only need to find a CCT value near CCT_{tar} instead of finding the local optimal value of CCT_{test}. It is worth noting that only three iterations are used for optimization when CCT_{tar} equals 3000 K, and the value of iterations increases with the increase in CCT_{tar}. This is because the initial values of A_B, A_Y, and A_R are very close to optimized values of A_B, A_Y, and A_R under low CCT_{tar}.

As we mentioned in Figure 3, different optimization results can be obtained under different CCT_{tar} with similar δ_1 and δ_2 values. To guarantee the achievement of the optimal Ra_{test} in all cases, we should initially manage to acquire optimized values for δ_1 and δ_2 (δ_{Opt1} and δ_{Op2}) under different CCT_{tar} values. It is worth noting that there exists a strong relationship between the sum of δ_{Opt1} and δ_{Opt2} ($\sum(\delta_{Opt1}, \delta_{Opt2})$) and CCT_{tar}. As shown in Figure 6, $\sum(\delta_{Opt1}, \delta_{Opt2})$ is plotted and fitted using a linear function under different CCT_{tar} values, which ranges from 3000 K to 12,000 K. It is evident that $\sum(\delta_{Opt1}, \delta_{Opt2})$ presents a perfect linear increasing trend with the increase in CCT_{tar}. The slope of this curve is calculated by using the linear interpolation method, and the curve can be described as

$$\sum(\delta_{Opt1}, \delta_{Opt2}) = \alpha \cdot CCT_{test} \quad (2)$$

where α is calculated to be 0.63 for the proposed WLED. For WLEDs combined with different light-conversion materials, the numerical value of α should be different. Additionally, the measured data slightly deviates from the fitting curve when CCT_{tar} equals 3000 K, which is probably because changes in δ_1 and δ_2 do not have visible effects on the optimization result when CCT_{tar} is low.

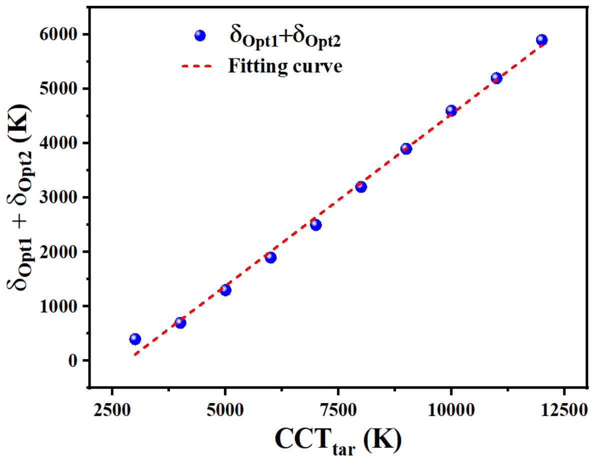

Figure 6. Data and fitting curve of $\sum(\delta_{Opt1}, \delta_{Opt2})$ under different CCT_{tar} values.

Once the law between α and light-conversion materials is identified, it is necessary to select the optimal δ_1 and δ_2 under different CCT_{tar} values before optimization. According to Figure 4, the optimal Ra_{test} corresponds to the largest δ_1 and δ_2 within the allowed range of CCT_{tar}. Except for the linear relationship between $\sum(\delta_{Opt1}, \delta_{Opt2})$ and CCT_{tar}, the value of δ_2 should be larger than δ_1, to guarantee the operation of the calculation procedure. Therefore, we had better select larger δ_2 and smaller δ_1 to satisfy Equation (2). This principle provides us with an effective way to accelerate the spectral optimization speed.

3.2. Comparison between the Proposed Method, Method I, and Method II

Tables 1–3 present calculation parameters of spectral optimization with the proposed method, method I, and method II. In Table 1, optimized CCT_{test} values are very close to CCT_{tar}. Among all results, the highest Ra_{test} reaches up to 96.1, with CCT_{test} of 4013 K. A_B, A_Y, and A_R exhibit a regular shifting trend in which A_B increases, and A_R reduces with the increase in CCT_{tar}. The sum of δ_1 and δ_2 increases with the increasing CCT_{tar}, which is consistent with the discussion and results in Figure 6. Optimization results of the proposed method and method I, in terms of CCT_{test}, Ra_{test}, A_B, A_Y, and A_R values, are highly coincident with each other. This coincidence verifies the correctness of the proposed method.

Table 1. Calculation parameters of spectral optimization using the proposed method.

CCT_{tar} (K)	CCT_{test} (K)	Ra	δ_{Opt1}	δ_{Opt2}	A_B	A_Y	A_R
3000	2924	95.1	200	200	0.11	0.30	0.47
4000	4013	96.1	400	300	0.33	0.30	0.30
5000	5011	94.2	1000	300	0.48	0.30	0.23
6000	6036	92.4	1600	300	0.60	0.30	0.20
7000	7018	90.8	2200	300	0.69	0.30	0.18
8000	8044	89.7	3000	200	0.75	0.30	0.15

Table 2. Calculation parameters of spectral optimization using method I.

CCT_{tar} (K)	CCT_{test} (K)	Ra	A_B	A_Y	A_R
3000	3059	95.3	0.12	0.30	0.46
4000	4013	96.1	0.33	0.30	0.30
5000	4908	94.3	0.46	0.30	0.23
6000	5927	92.7	0.57	0.30	0.18
7000	7011	90.8	0.69	0.30	0.17
8000	7950	89.8	0.72	0.30	0.13

Table 3. Calculation parameters of spectral optimization using method II.

CCT_{tar} (K)	CCT_{test} (K)	Ra	A_B	A_Y	A_R
3000	3013	95.5	0.13	0.30	0.47
4000	4041	96.0	0.34	0.30	0.30
5000	5007	94.1	0.49	0.30	0.24
6000	6047	91.8	0.62	0.30	0.21
7000	6924	87.2	0.58	0.30	0.07
8000	7917	85.6	0.65	0.30	0.05

In Table 3, calculation results of method II under low CCT_{tar} well match those of method I. Compared with the proposed method and method I, we can even obtain better optimization results of Ra_{test} under 3000 K by using method II. However, with the increase in CCT_{tar}, method II fails to effectively improve Ra_{test} to obtain the optimal value. Due to the random selection rule of method II, calculation results of A_B, A_Y, and A_R listed in Table 3 do not show a similar trend as in Tables 1 and 2. These results reveal that method II cannot effectively optimize WLED spectra under high CCTs. To apply A_B, A_Y, and A_R in a real scenario for realizing target illumination effects, ref. [24] presented the implementation method in detail.

By using Equation (2) to find δ_{Opt1} and δ_{Opt2} under different values of CCT_{tar}, we accelerate the optimization process. In Figure 7a, the number of iterations of these three methods under different values of CCT_{tar} is compared. Obviously, the number of iterations of the proposed method is much less than that of the other two methods. For the proposed method, the number of iterations increases with the increase in CCT_{tar}. The accuracy of CCT_{test} and Ra_{test} for these three methods can be evaluated by using the error range concept. Error ranges of CCT_{test} and Ra_{test} (ε_C and ε_R) are calculated by $|CCT_{tar} - CCT_{test}|/CCT_{tar}$ and $|100 - Ra_{test}|/100$, respectively. ε_C and ε_R under different values of CCT_{tar} are given in Figure 7b,c for comparison. The ε_C values of these three methods are comparable under different values of CCT_{tar}. The ε_R values of the proposed method and method I are similar, and they are relatively smaller than that of method II under high CCT_{tar} values. These results verify the effectiveness and accuracy of the proposed method.

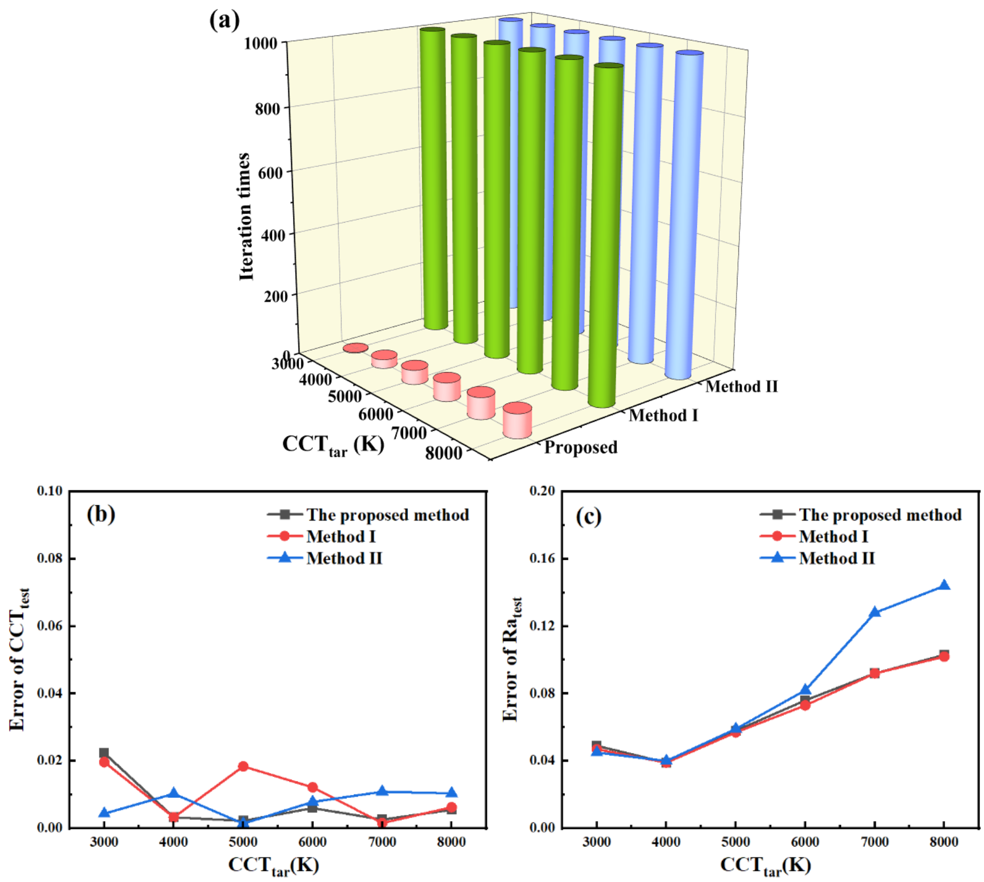

Figure 7. (**a**) Comparison between iteration times of the proposed method, method I, and method II, respectively, under different values of CCT_{tar}; (**b**,**c**) comparison between errors of CCT_{test} and Ra_{test} for the proposed method, method I, and method II, respectively, under different values of CCT_{tar}.

4. Conclusions

In this study, we propose an effective method to optimize the Ra of trichromatic WLEDs under different CCTs. Compared with conventional methods I and II, the proposed method exhibits superior searching ability to find the optimal Ra under target CCTs. Specifically, the highest Ra of 96.1 under 4013 K can be obtained after only 29 iterations. Three main mechanisms were investigated and analyzed for the proposed method: (1) the influence of δ_1 and δ_2 on the calculation results of CCT_m, CCT_{test}, and Ra_{test}; (2) the relationship between δ_1, δ_2, CCT_m, A_B, A_Y, and A_R; (3) the shifting rule of δ_{Opt1} and δ_{Opt2} under different CCT_{tar} values. Particularly, the fitting linear curve that describes the relationship between $\sum(\delta_{Opt1}, \delta_{Opt2})$ and CCT_{tar} can provide an effective way to greatly accelerate the optimization process under different CCT_{tar} values. This study reveals the shifting mechanism of CCT and Ra values with dual-weight coefficients and greatly enhances the effectiveness of spectral optimization for WLEDs. Our method is hopefully applied in related areas such as residential intelligent lighting and smart planting LED systems.

Author Contributions: Conceptualization, H.X.; methodology, H.X. and Y.L.; formal analysis, H.X. and Y.L.; writing—original draft preparation, H.X. and B.L.; writing—review and editing, Y.L., B.L., and G.W. All authors have read and agreed to the published version of the manuscript.

Funding: This research was supported by the Youth Talent Program of the Education Department of Guangdong Province (Number: 2020KQCX026).

Acknowledgments: The authors would like to thank the Academy for Advanced Interdisciplinary Studies, Department of Electrical and Electronic Engineering, Southern University of Science and Technology, for their technical assistance.

Conflicts of Interest: The authors declare no conflict of interest.

References

1. Su, Z.; Zhao, B.; Gong, Z.; Peng, Y.; Bai, F.; Zheng, H.; Joo, S.W. Color-tunable white LEDs with single chip realized through phosphor pattern and thermal-modulating optical film. *Micromachines* **2021**, *12*, 421. [CrossRef]
2. Zhao, S.; Cai, W.; Wang, H.; Zang, Z. Inorganic lead-free cesium copper chlorine nanocrystal for highly efficient and stable warm white light-emitting diodes. *Photonics Res.* **2020**, *9*, 187–192. [CrossRef]
3. Wang, H.; Xing, Y.H.; Li, J.X.; Tan, J.; Li, Z.T.; Song, C.H.; Li, J.S. Highly efficient lquid-quantum dot/melamine-modified urea-formaldehyde microcapsules for white light-emitting diodes. *IEEE Electron Device Lett.* **2021**, *42*, 533–536. [CrossRef]
4. Chiang, C.H.; Gong, S.J.; Zhan, T.S.; Cheng, K.C.; Chu, S.Y. White light-emitting diodes with high color rendering index and tunable color temperature fabricated using separated phosphor layer structure. *IEEE Electron Device Lett.* **2016**, *37*, 898–901. [CrossRef]
5. Zhong, P.; He, G.; Zhang, M. Spectral optimization of the color temperature tunable white light-emitting diode (LED) cluster consisting of direct-emission blue and red LEDs and a diphosphor conversion LED. *Opt. Express* **2012**, *20*, A684–A693. [CrossRef]
6. Wu, T.; Lin, Y.; Zhu, H.; Guo, Z.; Zheng, L.; Lu, Y.; Shih, T.M.; Chen, Z. Multi-function indoor light sources based on light-emitting diodes—A solution for healthy lighting. *Opt. Express* **2016**, *24*, 24401–24412. [CrossRef]
7. Arellano-Morales, A.; Molina-González, J.; Desirena, H.; Bujdud-Perez, J.M.; Calixto, S. High CRI in phosphor-in-doped glass under near-ultraviolet excitation for warm white light-emitting diode. *J. Lumin.* **2021**, *229*, 117684. [CrossRef]
8. Murad, M.A.; Razi, K.; Jeong, B.R.; Samy, P.M.A.; Muneer, S. Light emitting diodes (LEDs) as agricultural lighting: Impact and its potential on improving physiology, flowering, and secondary metabolites of crops. *Sustainability* **2021**, *13*, 1985. [CrossRef]
9. Nii, K.; Okada, H.; Itoh, S.; Kusaka, T. Characteristics of bilirubin photochemical changes under green light-emitting diodes in humans compared with animal species. *Sci. Rep.* **2021**, *11*, 6391. [CrossRef]
10. Petr, C.; Andrew, B.; Petr, P.; Li, X. Visible light communications: Increasing data rates with polarization division multiplexing. *Opt. Lett.* **2020**, *45*, 2977–2980.
11. Alatawi, A.A.; Holguin-Lerma, J.A.; Kang, C.H.; Shen, C.; Subedi, R.C.; Albadri, A.M.; Allyamani, A.Y.; Ng, T.K.; Ooi, B.S. High-power blue super luminescent diode for high CRI lighting and high-speed visible light communication. *Opt. Express* **2018**, *26*, 26355–26364. [CrossRef]
12. Guo, Z.; Shih, T.M.; Lu, Y.; Gao, Y.; Zhu, L.; Chen, G.; Zhang, J.; Lin, S.; Chen, Z. Studies of scotopic/photopic ratios for color-tunable white light-emitting diodes. *IEEE Photonics J.* **2013**, *5*, 8200409. [CrossRef]
13. Wei, M.; Yang, B.; Lin, Y. Optimization of a spectrally tunable LED daylight simulator. *Color Res. Appl.* **2017**, *42*, 419–423. [CrossRef]
14. Zhu, P.; Zhu, H.; Adhikari, G.C.; Thapa, S. Spectral optimization of white light from hybrid metal halide perovskites. *OSA Contin.* **2019**, *6*, 1880–1888. [CrossRef]
15. Titkov, I.E.; Yadav, A.; Karpov, S.Y.; Sakharov, A.V.; Tsatsulnikov, A.F.; Slight, T.J.; Gorodetsky, A.; Rafailov, E.U. Superior color rendering with a phosphor-converted blue-cyan monolithic light-emitting diode. *Laser Photonics Rev.* **2016**, *10*, 1031–1038. [CrossRef]
16. Yuan, B.; Guan, S.; Sun, X.; Li, X.; Zeng, H.; Xie, Z.; Chen, P.; Zhou, S. Highly efficient carbon dots with reversibly switchable green−red emissions for trichromatic white light-emitting diodes. *ACS Appl. Mater. Interfaces* **2018**, *10*, 16005–16014. [CrossRef]
17. Song, B.M.; Han, B. Spectral power distribution deconvolution scheme for phosphor-converted white light-emitting diode using multiple Gaussian functions. *Appl. Opt.* **2013**, *52*, 1016–1024. [CrossRef]
18. Carli, N.; Sperling, A.; Bizjak, G. Optimization methods for spectral synthesizing of a tuneable colour light source. *Light Eng.* **2018**, *26*, 99–108. [CrossRef]
19. Birgin, E.G.; Martínez, J.M.; Raydan, M. Spectral projected gradient methods: Review and perspectives. *J. Stat. Softw.* **2016**, *60*, 1–21. [CrossRef]
20. Zielonka, A.; Sikora, A.; Wozniak, M.; Wei, W.; Ke, Q.; Bai, Z. Intelligent internet of things system for smart home optimal convection. *IEEE Trans. Ind. Inform.* **2020**, *17*, 4308–4317. [CrossRef]
21. Blanco, J.; García, A.; Morenas, J.D.L. Design and implementation of a wireless sensor and actuator network to support the intelligent control of efficient energy usage. *Sensors* **2018**, *18*, 1892. [CrossRef] [PubMed]
22. Qiang, Y.; Yu, Y.; Chen, G.; Fang, J. A flux-free method for synthesis of Ce^{3+}-doped YAG phosphor for white LEDs. *Mater. Res. Bull.* **2016**, *74*, 353–359. [CrossRef]
23. Pu, C.; Peng, X. To battle surface traps on CdSe/CdS core/shell nanocrystals: Shell isolation versus surface treatment. *J. Am. Chem. Soc.* **2016**, *138*, 8134–8142. [CrossRef] [PubMed]

24. Xiao, H.; Xiao, X.; Wang, K.; Wang, R.; Xie, B.; Chiang, K.S. Optimization of illumination performance of trichromatic white light-emitting diode and characterization of its modulation bandwidth for communication applications. *IEEE Photonics J.* **2018**, *10*, 8201511. [CrossRef]
25. Erdem, T.; Nizamoglu, S.; Sun, X.W.; Demir, H.V. A photometric investigation of ultra-efficient LEDs with high color rendering index and high luminous efficacy employing nanocrystal quantum dot luminophores. *Opt. Express* **2010**, *18*, 340–347. [CrossRef]